Journal of Polymers and the Environment (2019) 27:510–520
https://doi.org/10.1007/s10924-019-01367-5

ORIGINAL PAPER

Nanocomposites Based on Poly(lactic acid) and Bacterial Cellulose Acetylated by an α-Hydroxyacid Catalyzed Route

Jhon Alejandro Ávila Ramírez[1,2,3] · Patricia Cerrutti[2,4] · Celina Bernal[3,5] · María Inés Errea[1] · María Laura Foresti[2,3]

Published online: 14 January 2019

Abstract
Poly(lactic acid) (PLA) nanocomposite films reinforced with acetylated bacterial cellulose nanoribbons were prepared by solvent casting. Acetylation of bacterial cellulose (BC) was performed by an innovative and sustainable direct solvent-free route catalyzed by citric acid. The effect of derivatization and its extent on the morphological, optical, thermal and mechanical properties of the nanocomposites was analyzed. Data collected from the above studies showed that acetylation of BC nanoribbons clearly improved the nanofibers dispersion in the PLA matrix with respect to unmodified BC, which in turn resulted in increased transparency and mechanical properties of the nanocomposites produced.

Keywords Bacterial cellulose · Acetylation · Citric acid · Poly(lactic acid) · Nanocomposites

Introduction

In the context of the current concern for the environment, the use of biodegradable polymers derived from natural resources deserves great attention from academy, industry and consumers. Among biobased polymers, poly(lactic acid) (PLA), a biodegradable aliphatic thermoplastic polyester, has a number of characteristics which make it unique in the marketplace. In the first place, the starting material, lactic acid, can be produced by fermentation of 100% annually renewable resources. Besides, PLA can be designed to controllably biodegrade, with a CO_2 generation balanced by the amount taken from the atmosphere during the growth of plant feedstocks. Apart from its origin and biodegradability, the wide application of PLA in packaging, paper coating, fibers, films, and molded articles is mainly based on its high modulus, high strength and transparency; being in many applications (e.g. food packaging) a cost-effective alternative to commodity petrochemical-based plastics. Depending on the stereopurity of the polymer backbone, PLA can be semi-crystalline or totally amorphous. PLA can be stress crystallized, thermally crystallized, impact modified, filled, copolymerized, and processed in most polymer processing equipment. It can also be formed into transparent films, fibers, or injection molded into blow moldable preforms for bottles [1].

In the last years, a number of contributions have dealt with the reinforcement of PLA with cellulose nanocrystals [2–5], and cellulose nanofibers from vegetal [6–10] and microbial sources [11–14]. The aim of these contributions has been mainly to prepare totally biodegradable nanocomposites with reduced water vapor permeability and oxygen transmission rate, and/or enhanced thermal and mechanical properties. However, the high surface area and hydrophilic nature of nanocelluloses often leads to poor dispersibility/compatibility with nonpolar media, resulting in inefficient compounding with most nonpolar polymeric matrices in which repulsive forces lead to aggregation

✉ María Laura Foresti
mforesti@fi.uba.ar

1 Centro de Ingeniería del Medio Ambiente (CIMA), Instituto Tecnológico de Buenos Aires (ITBA), Av. Eduardo Madero 399, CP 1106ACD Buenos Aires, Argentina

2 Grupo de Biotecnología y Biosíntesis, Facultad de Ingeniería, Instituto de Tecnología en Polímeros y Nanotecnología (ITPN-UBA-CONICET), Universidad de Buenos Aires, Las Heras 2214, CP 1127AAR Buenos Aires, Argentina

3 Consejo Nacional de Investigaciones Científicas y Técnicas (CONICET), Buenos Aires, Argentina

4 Departamento de Ingeniería Química, Facultad de Ingeniería, Universidad de Buenos Aires, Buenos Aires, Argentina

5 Grupo de Propiedades Mecánicas y Fractura, Facultad de Ingeniería, Instituto de Tecnología en Polímeros y Nanotecnología (ITPN-UBA-CONICET), Universidad de Buenos Aires, Las Heras 2214, CP 1127AAR Buenos Aires, Argentina

and poor interfacial contact. To overcome this problem, lately, most contributions dealing with PLA/nanocellulose composites have incorporated the use of amphiphilic surfactants or previous steps devoted to chemical modification or grafting of nanocellulose [15–33]. In terms of chemical modification options, the possibility of conferring a hydrophobic character only to the surface of cellulose nanofibers/nanocrystals, while keeping the integrity of their crystalline core unchanged, is a challenge that has been triggering much research [34].

In the current contribution, bacterial cellulose (BC) was used as reinforcement of PLA. Chemically identical to plant cellulose, BC is recognized for its naturally occurring nanometric dimensions and its high purity, as it is obtained free of lignin, hemicelluloses, and pectins found in lignocellulosic materials. BC is also characterized by high transparency, a high degree of polymerization (i.e., 2000–10,000 anhydroglucose units), high crystallinity, tunable porosity, high elasticity and mechanical stability, light weight, renewability, biodegradability, indigestibility in the human intestinal tract, high liquid loading capacity, high degree of conformability, biocompatibility, non-toxicity, non-pyrogenicity, and extensive surface area [35, 36].

BC has been previously used as reinforcement of different polymeric matrices with promising results [37, 38]. In this context, and in order to broaden the uses of BC as reinforcement of nonpolar matrices, a number of chemical methodologies devoted to hydrophobize the surface of BC, mainly by esterification of exposed hydroxyl groups, have been reported [28, 30, 39–52]. Although generally efficient for attaining the hydrophobization extent required, most acetylation methodologies reported to derivatize BC relay on the use of highly corrosive strong acids as catalysts (e.g. perchloric or sulphuric acids), and/or involve media containing highly flammable or toxic organic solvents such as pyridine or toluene. On the other hand, previous contributions of some of us have recently referred to a non-conventional acetylation protocol of BC performed in the absence of cosolvents and catalyzed by naturally occurring α-hydroxy acids, which succeeded in reducing the hydrophilic character of BC nanoribbons surface while keeping the ultrastructure of BC intact [53–55]. The intrinsic benefits of the route proposed include the natural origin of the catalysts used (e.g. lactic, tartaric and citric acid) which can be produced at large scale by biotechnological routes, their non-toxic and biodegradable character, and the fact that no cosolvent is used [56]. In the present work, surface acetylated BC obtained by esterification catalyzed by citric acid with varying derivatization extents was used as reinforcement of PLA for the first time. Morphological, optical, thermal and mechanical characterization of the obtained nanocomposites is provided.

Experimental

Materials

Commercial PLA (3051D, Nature Works®) with a molecular weight (M_n) of *ca.* 1.42×10^4 g/mol, a specific gravity of 1.24 and a melt flow index (MFI) of 7.75 g/10 min (210 °C, 2.16 kg) [16] was used as the matrix of the nanocomposites. PLA pellets were dried at 98 °C for 3 h under vacuum before use. Bacterial cellulose (BC) was produced in static culture using the bacterial strain *Gluconacetobacter xylinus*, NRRL B-42. The culture medium was formulated using anhydrous dextrose (Biopack), meat peptone (Britania, Laboratorios Britania S.A.), yeast extract (Britania, Laboratorios Britania S.A.), disodium phosphate (Anedra), citric acid (Merck), glycerol (Sintorgan) and corn steep liquor (Ingredion). Acetic anhydride (Cicarelli), acetic acid (Cicarelli), citric acid (Merck), hydrochloric acid (Cicarelli), sodium hydroxide (Biopack), acetone (Sintorgan) and chloroform (Cicarelli), were all reagent grade chemicals which were used as received.

Bacterial Cellulose Production

BC was produced in static culture using a *Gluconacetobacter xylinus* strain under previously optimized conditions [57]. Briefly, the inocula of *G. xylinus* NRRL B-42 were cultured in 100 mL Erlenmeyers flasks containing 20 mL of Hestrin and Schramm (HS) medium [58] and incubated with orbital agitation (200 rpm) for 48 h at 28 °C. For BC production, 1% (v/v) inocula were transferred to 10 L steel trays with 5.0 L of fermentation medium containing 4.0wt% glycerol and 8.0wt% corn steep liquor, and statically incubated at 28 °C during 14 days. Pellicles were then harvested, thoroughly rinsed with distilled water to remove the culture medium, and homogenized in a blender in KOH solution (5% w/v) for 5 min. The suspension was left in alkali at room temperature for 14 h to eliminate the bacterial cells, and finally rinsed with distilled water till neutralization.

Citric acid-catalyzed acetylation of BC

Homogenized BC pellicles (0.5 g dry weight) were solvent exchanged from water through acetic acid into acetic anhydride, using 20 mL each time. The solvent exchanged BC was then contacted with citric acid (0.34 mmol/mmol AGU) and 50 mL of acetic anhydride in a 100 mL glass flask equipped with a reflux condenser. The mixture was then heated to 120 °C under continuous magnetic agitation in a thermostatized oil bath. The level of acetylation of BC was modulated by manipulation of reaction time (0.5, 2.0,

and 5.0 h). After those reaction intervals, the derivatized BC was separated by vacuum filtration and thoroughly washed with ethanol and distilled water.

The level of esterification conferred to BC was determined by heterogeneous saponification and back titration with HCl, as detailed elsewhere [53]. The acyl content and the degree of substitution (DS, i.e. average number of substituted hydroxyl groups per anhydroglucose unit (AGU), maximum value = 3) achieved were then calculated as stated in Eqs. (1) and (2), respectively:

$$\text{Acyl}(\%) = [(V_B - V_S) \times N_{HCl} \times 4.3]/W \quad (1)$$

$$DS = \frac{(162 \times \text{Acyl}\%)}{[4300 - (42 \times \text{Acyl}\%)]} \quad (2)$$

where V_B (ml) is the volume of HCl required for blank titration, V_S (mL) is the volume of HCl required to titrate the sample, N_{HCl} is the normality of the HCl solution, and W (g) is the mass of sample used.

Preparation of PLA/BC nanocomposites

Native and acetylated BC with different DS were solvent exchanged from water through acetone (twice) into chloroform (twice). In each step, samples were homogenized at 18,000 rpm using an Ultra Turrax D160 handheld homogenizer.

PLA nanocomposite films were prepared by solvent casting. For the neat PLA film, 2 g of PLA were dissolved in 65 mL of chloroform with magnetic stirring (RT, 1000 rpm, 3 h). Subsequently, the PLA solution was poured onto a 90 mm glass Petri dish and allowed to dry for 48 h at RT. For the nanocomposite films, the PLA solution previously prepared was mixed with BC and acetylated BC suspensions (0.06 g, dry weight) in chloroform to a final reinforcement content of 3 wt % (chosen as an intermediate value from previous contributions dealing with PLA reinforced with BC [14, 28, 30]). The mixtures were homogenized at 18,000 rpm for 15 min before they were casted onto glass Petri dishes following the same protocol used for neat PLA. All films were placed in a vacuum oven at 40 °C for 4 weeks before characterization in order to remove the remaining chloroform. Films obtained had a nominal thickness of ≈ 250 µm.

Characterization

Transmission electron microscopy (TEM)

Aiming to illustrate its nanofibrillar nature, drops of a diluted aqueous suspension of BC were deposited onto glow-discharged carbon-coated electron microscopy grids and negatively stained with 2 wt% uranylacetate. Samples were observed using a TEM Philips EM 301 microscope operating at an acceleration voltage of 40 kV.

Field Emission Scanning Electron Microscopy (FESEM)

Drops of diluted aqueous suspensions of native and acetylated BC (0.2wt%) were deposited on microscope glasses and dried at 100 °C for 5 min. For the PLA/BC nanocomposites cryo-fractured cross sections of the specimens obtained at liquid nitrogen temperature were analyzed. All samples were sputtered coated with a thin layer of gold before observation in a scanning electron microscope Zeiss Supra 40 with field emission at an accelerating voltage of 3 kV.

Fourier Transform Infrared Spectroscopy (FTIR)

Fourier transform infrared spectra of native and acetylated grinded BC samples were acquired on an IR Affinity-1 Shimadzu Fourier Transform Infrared Spectrophotometer in absorbance mode. Carefully dried (12.5 mg, 110 °C, 1 h) samples were mixed with previously dried KBr (130 °C, overnight) at 1:20 ratio and pressed into a disc. Samples were scanned 40 times at a resolution of 4 cm^{-1} in the range of 4000 to 700 cm^{-1}. The derived spectra were baseline corrected and normalized against the intensity of the absorption at 1165 cm^{-1}, corresponding to the (C–O–C) link of cellulose [48, 59].

Solid-State Nuclear Magnetic Resonance Spectroscopy (CP/MAS ^{13}C NMR)

High-resolution ^{13}C solid-state spectra of native and acetylated grinded BC samples were collected using the ramp {1H} → {13C} CP/MAS pulse sequence with proton decoupling. ^{13}C NMR spectra were collected in a Bruker Avance II-300 spectrometer equipped with a 4-mm MAS probe at room temperature. The operating frequency for protons and carbons was 300.13 and 75.46 MHz, respectively. Glycine was used as an external reference for the ^{13}C spectra and to set the Hartmann-Hahn matching condition in the cross-polarization experiments. The recycling time varied from 5 to 6 s, and the contact time during CP was 2 ms. The SPINAL64 sequence (small phase incremental alternation with 64 steps) was used for heteronuclear decoupling during acquisition with a proton field H1H satisfying $\omega 1H/2\pi = YHH1H = 62$ kHz. The spinning rate for all the samples was 10 kHz.

X-ray Diffraction Analysis (XRD)

The structure of native and acetylated BC, and PLA/BC nanocomposites was analyzed with a Rigaku D/Max-C Wide Angle automated X-ray diffractometer with

vertical goniometer operating with a Cu/Kα radiation source (0.154 nm) at 40 kV and 30 mA. The X-ray diffraction pattern was recorded in the 10-45° 2θ interval at a step size of 0.02°. The crystallinity index of BC samples was estimated from diffraction intensity data by use of Segal's empirical equation [60], where I_{002} corresponds to the maximum intensity of the 002 lattice diffraction and accounts for both crystalline and amorphous material, and I_{am} is the intensity at 2θ = 18° which represents amorphous material only.

$$CI = \frac{(I_{002} - I_{am})}{I_{002}} \times 100 \quad (3)$$

The crystallinity fraction of the nanocomposite films was determined based on the ratio of the crystalline peaks area and the total diffractogram area.

Optical Properties

The transparency of the nanocomposite films was determined both qualitatively, by the assessment of their contact transparency; and quantitatively by recording of their transmittance in the 200–800 nm range using a Shimadzu UV/visible spectrophotometer (Model UV-1650 pc). Due to the films-thickness inhomogeneities, spectra were recorded in at least three different positions within the films.

Differential Scanning Calorimetry (DSC)

Thermal analysis of neat PLA and PLA/BC nanocomposites was carried out in a differential scanning calorimeter (DSC) Shimadzu DSC- 60. A first heating scan from 25 °C to 200 °C at 10°C/min was applied. Samples were then kept at 200 °C for 2 min in order to erase any thermal history, and further cooled from 200 °C to -25 °C at 10°C/min. A second heating scan from − 25 °C to 200 °C at 10°C/min was applied. Cold crystallization (T_{cc}) and melting (T_m) temperatures were determined as the maximum of the exothermic and endothermic signals, respectively. Glass transition temperature values (T_g) were obtained from the cooling scan. The degree of crystallinity of the casted films was calculated from the first heating scan using Eq. 4, where the w_{PLA} is the weight fraction of PLA in the sample and ΔH_{m0} is the enthalpy of melting for a 100% crystalline PLA sample taken as 93.6 J/g [61]:

$$X = \frac{1}{W_{PLA}} \left(\frac{\Delta H_m}{\Delta H_{m0}} \right) \times 100 \quad (4)$$

Mechanical Characterization

Uniaxial tensile tests were carried out on type IV (ASTM D638) dumbbell samples cut out from the PLA matrix and the PLA/BC nanocomposites films in an INSTRON dynamometer 5982 at a crosshead speed of 1 mm/min and using a load cell of 1 KN. Stress–strain curves were obtained from these tests, and tensile parameters values (Young's modulus, tensile strength, and strain at break) were determined from the curves. The measurements were performed at room temperature and at least five samples for each material were tested. Average values and their deviations were reported.

Results and Discussion

Production and Characterization of Nanofillers

In static culture bacterial cellulose is obtained as an entangled nanoribbons network grown in the air–liquid interface of the fermentation vial. Although a relatively great number of microorganisms can synthetize cellulose, few species are reported to produce it in good yields compatible with large scale fermentations, as it is the case of *Gluconacetobacter xylinus* (formerly, *Acetobacter xylinum*, now syn. *Komagataeibacter xylinus*), the strain used herein to produce BC. BC cellulose ribbon biogenesis is recognized as a hierarchical, cell-directed self-assembly process [62], in which subelementary fibrils of a lateral width of ≈ 1.5 nm composed of 12–15 cellulose chains produced by cellulose synthases enzymes, aggregate to form first microfibrils of ≈ 3–6 nm in width and then typical ribbons with a lateral width of 40–60 nm [63]. Figure 1a is a photograph of a BC pellicle obtained under the conditions set, whereas Fig. 1b shows a TEM image of a diluted BC suspension obtained after 5 min of homogenization in a blender. The histogram in Fig. 1c shows the distribution of nanoribbons widths determined from TEM images.

Homogenized BC pellicles were acetylated by means of a non-conventional methodology relaying on the use as catalyst of a naturally occurring α-hydroxy acid such as citric acid. Acetylation was performed in the absence of cosolvents, following previously optimized conditions [55] summarized in "Citric acid-catalyzed acetylation of BC" section. These protocols have proved to result in surface hydrophobization of BC ribbons with no detectable concomitant citric acid grafting or induced crosslinking [53–55]. The extent of esterification expressed as the degree of substitution (DS) was herein tuned by manipulation of reaction time, keeping all other reaction conditions constant ("Citric acid-catalyzed acetylation of BC" section). Acetylation carried out during 0.5, 2.0 and 5.0 h led to DS values of 0.25, 0.43 and 0.61, respectively.

Figure 2 collects ^{13}C NMR, FTIR, XRD and FESEM data from native BC and acetylated BC samples. Introduction of acetate groups in BC was confirmed by CP/MAS ^{13}C NMR

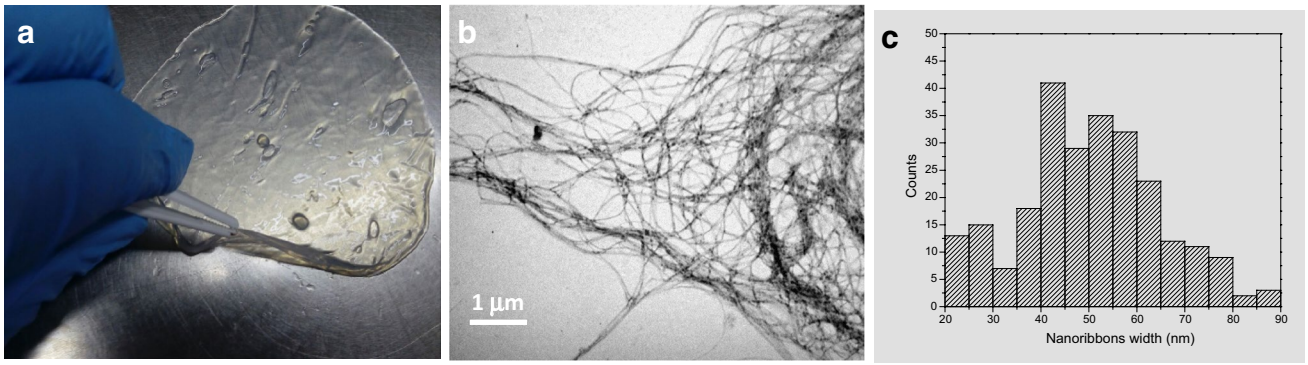

Fig. 1 **a** BC pellicle obtained with *G. xylinus*, **b** TEM image of negatively stained BC nanoribbons and **c** corresponding histogram (width)

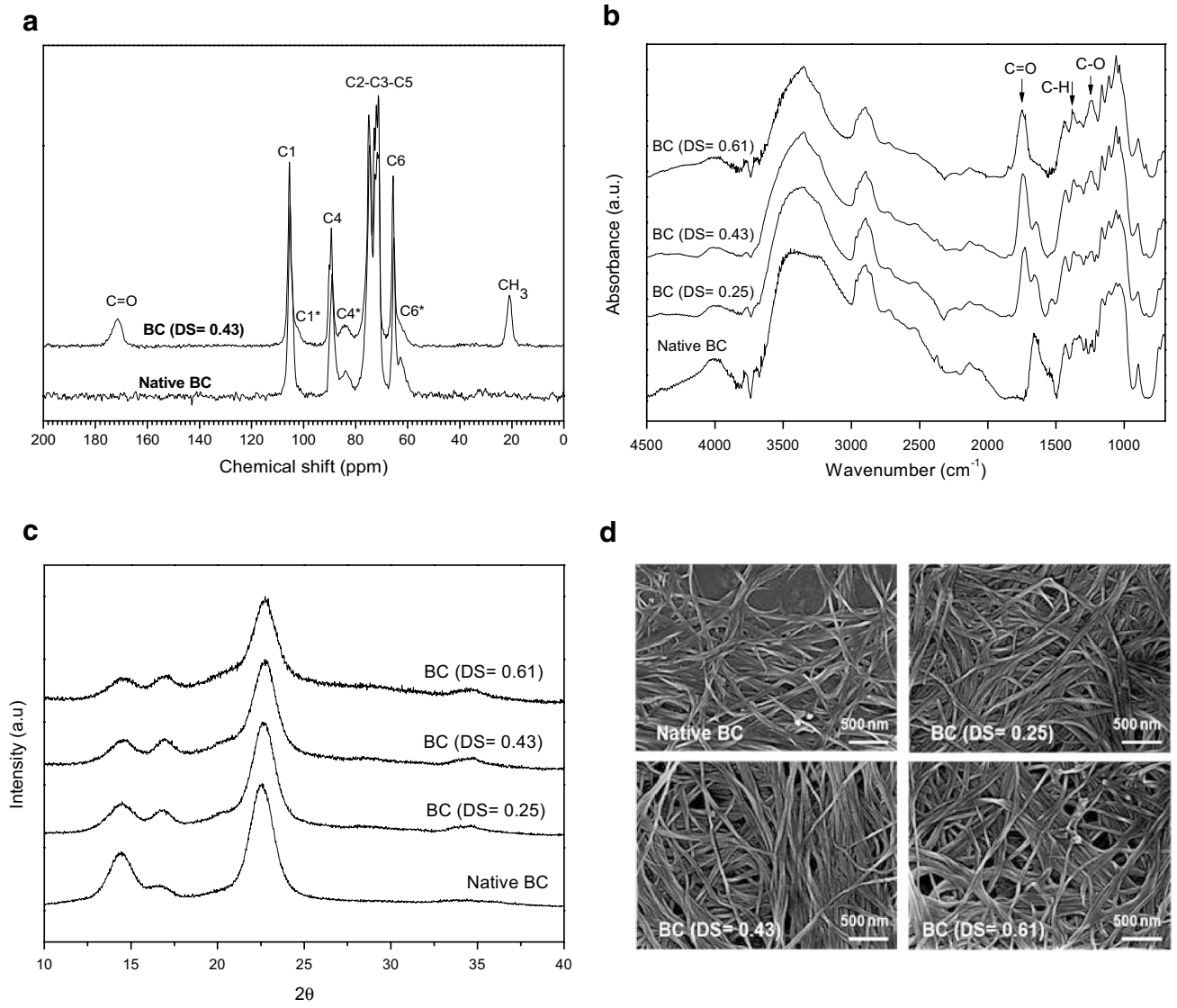

Fig. 2 Native and acetylated BC samples characterization. **a** CP/MAS ^{13}C NMR spectra, **b** FTIR spectra, **c** X-ray diffraction patterns, **d** SEM micrographs

spectroscopy of derivatized samples (Fig. 2a) by appearance of two new resonances centered at 21 ppm and 172 ppm assigned to the methyl and carbonyl carbons of the acetate group, respectively. Besides, the absence of resonances at ≈44 ppm indicated no detectable citric acid presence either as impurity or esterified onto BC. In FTIR spectra (Fig. 2b), the appearance of new signals typical of ester groups, i.e. 1745 cm^{-1} due to C=O stretching, and 1243 cm^{-1} due to C–O stretching, was also considered a diagnostic of esterification. The X-ray diffraction profiles of native and acetylated BC are presented in Fig. 2c. The diffraction peaks typical of cellulose I were observed centered at 2θ = 14.4° (101), 16.7° (10–1) and 22.6° (002). As observed previously by other authors dealing with surface-only BC acetylation [45, 48], acetylation showed to induce some modification in the relative area of the crystalline peaks centered at 14.4° and 16.7°. Crystallinity index (CI) values were calculated using the Segal equation after baseline subtraction of the spectrum. As it is shown, the acetylation levels conferred to the BC samples had a minor effect on crystallinity, i.e. 91% for DS = 0.25, 89% for DS = 0.43, 86% for DS = 0.61, versus 92% for native BC. The previous suggests that the citric acid-catalyzed acetylation of BC performed was mainly a surface phenomenon which did not affect the ultrastructure of the nanofibers. FESEM images of native and acetylated BC samples are shown in Fig. 2d. Micrographs illustrate that acetylation induced no significant changes on the fibrils surface, with the web-like fibrous structure typical of BC being preserved even for the highest DS value conferred.

Nanocomposites Characterization

Native BC and acetylated BC were used as reinforcement of PLA at 3 wt%. Figure 3a collects the photographs of the films obtained, evidencing the effect of acetylation on the relative dispersion of the nanofiller within the matrix.

While the PLA film is transparent, in the PLA/native BC film aggregates of bacterial cellulose are clearly evident to the naked eye. This indicates that poor dispersion of unmodified BC into PLA was obtained in spite of the homogenization included in all the steps of composites preparation, and also despite the use of never dried BC aimed at avoiding extensive self-association of cellulose nanoribbons through hydrogen bonding during drying processes. Poor dispersion of unmodified BC results from incompatibility between hydrophilic BC and less polar PLA, which leads to aggregation of nanofibers and poor interfacial contact. On the other hand, nanocomposites derived from acetylated BC were much more homogenous, suggesting that acetylation resulted in improved compatibility with the matrix and better dispersion of the nanofiller. Significant improvements in BC dispersion in PLA upon acetylation by other routes have been reported previously [30].

The relative contact transparency of the films obtained is further illustrated in Fig. 3b. The nanocomposite resulting from unmodified BC shows reduced transparency when compared with pure PLA, whereas the transparency of acetylated BC-PLA films recalls that of the matrix. The results can be explained in terms of the better dispersion of cellulose nanofibers upon derivatization described before, which resulted in reduced scattering. Analysis of the light transmittance in the wavelength from 200 to 800 nm further confirmed the previous observations. As exemplified in Fig. 3c, the film containing the derivatized BC led to a transmittance curve much closer to that of the neat PLA film than that of PLA/Native BC.

Figure 4 shows FESEM micrographs of cryogenic fracture surfaces of the different nanocomposite films investigated. In accordance with transparency results, in Fig. 4a native BC nanoribbons highly aggregated within the PLA matrix were clearly observed. Nanocomposites containing modified BC, on the other hand, presented less distinguishable nanoribbons and improved morphology. Better filler dispersion may be associated with higher compatibility of BC with the PLA matrix as a consequence of derivatization, as previously observed for PLA/BC nanocomposites including BC acetylated by other routes [30, 31]. On the other hand, no significant differences in nanofiller dispersion were observed among the three substitution degrees investigated.

Figure 5 shows the DSC thermograms of neat PLA and the different nanocomposites obtained. Upon first heating (Fig. 5a), neat PLA and their nanocomposites only presented an endothermic melting peak (T_m and ΔH_m values are presented in Table 1). No significant changes neither in the melting enthalpy nor in the melting temperature among the different materials investigated were observed. In addition, for all films crystallinity (X) values were in the 35–37% interval, suggesting that the incorporation of the nanofillers did not significantly affect the degree of crystallinity of the matrix. Similar results have been previously reported for other PLA/BC systems [28]. During cooling (Fig. 5b), no crystallization peak was observed neither in the neat PLA matrix nor in the composites including derivatized BC. PLA is a slow crystallization polymer and, in order to induce crystallization, relatively low cooling rates are often required [13]. However, when neat BC was used as filler, a small crystallization peak appeared in the cooling curve centered at 96 °C, suggesting that the unmodified BC aided PLA crystallization. On the other hand, a glass transition temperature close to 59 °C could be detected independently of the system. During the second heating (Fig. 5c), no exothermic peak attributed to the cold crystallization occurred in neat PLA. Contrarily, the nanocomposite with native BC did show an exothermic peak followed by the melting endothermic peak, further implying that this filler aided PLA crystallization by acting as a nucleating agent as previously

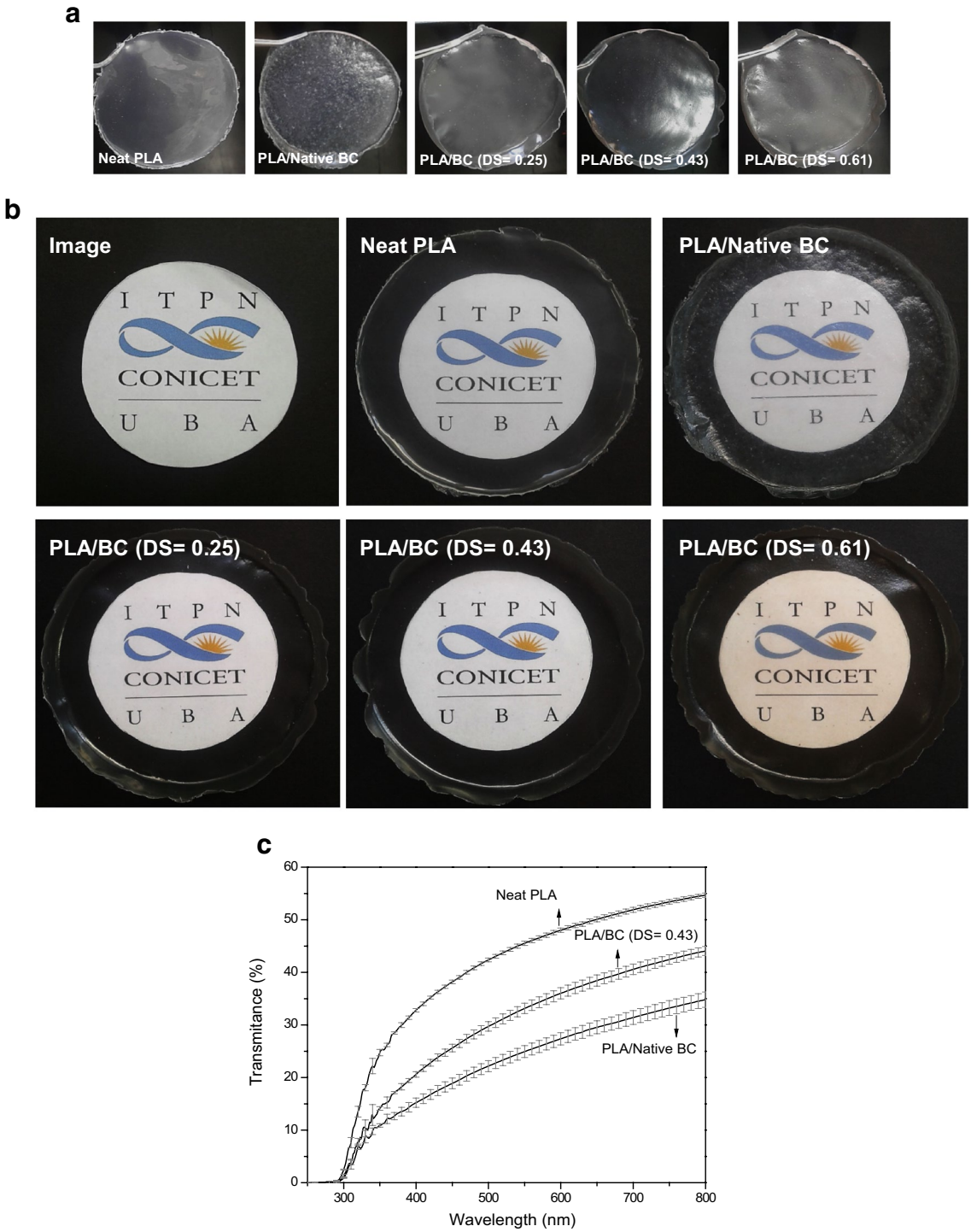

Fig. 3 **a, b** Photographs of neat PLA and nanocomposite films illustrating their transparency. **c** Films transmittance spectra

observed by others for similar systems [12–14, 28, 64]. On the other hand, on second heating the composite with the less acetylated BC (i.e. DS = 0.25) led to much less intense crystallization and melting peaks, and higher cold crystallization temperature values (Table 1). The magnitude of both peaks increased with the acetylation extent conferred to BC. Besides, lower (but still higher than the native BC counterpart) cold crystallization temperature values were observed as BC with higher DS was used as filler. Evidently, the chemical nature of BC surface, -and thus its dispersibility and relative compatibility with the hydrophobic PLA matrix-, played a key role in controlling PLA crystallization

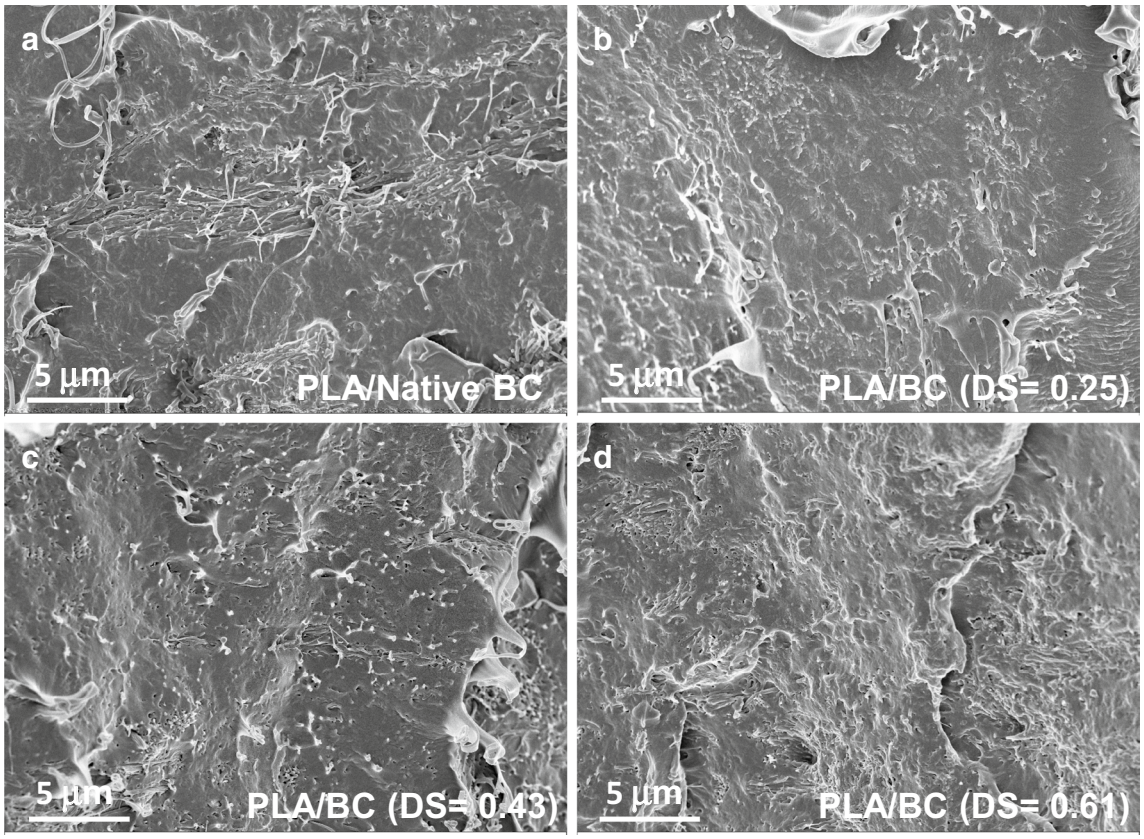

Fig. 4 SEM micrographs of cryogenic fracture surfaces of nanocomposites with different reinforcements. **a** Native BC, **b** DS 0.25, **c** DS 0.43, **d** DS 0.61

feasibility. The previous is probably a consequence of counteracting phenomena associated to hindered diffusion and folding of the PLA chains as a result of compatibilization, and nucleation effects induced by relative dispersion of the fillers.

The structure of the different nanocomposite films was analyzed by XRD (Fig. 6). PLA exhibited a strong crystalline peak at $2\theta = 16.8°$ and a weaker peak at 19.2°, in accordance with diffractograms of other semycristalline PLAs [65, 66]. Minor peaks at $2\theta = 15.0°$ and 22.4° were also observed in the diffractogram of neat PLA. On the other hand, native and acetylated BC with varying DS have a typical cellulose I structure with three well-defined diffraction peaks centered at $2\theta = 14.4°$ (101), 16.7° (10 − 1) and 22.6° (002). However, the characteristic peaks of BC could not be observed in the X-ray diffraction patterns of the nanocomposites, not even the most intense BC peak at 22.5°, due to the overlapping with PLA crystalline peaks. This result differs from previous contributions in which a more amorphous nature of the PLA used allowed the observation of BC crystalline peaks, especially as higher nanofiller contents were assayed [11, 27]. In terms of the degree of crystallinity of the films analyzed, and in accordance with DSC results, neither neat BC nor acetylated BC had a significant effect on the nanocomposites crystallinity, with X (%) values in the 36–41% interval for all samples. Moreover, comparison of nanocomposites XRD patterns with that of neat PLA, showed no other effect of the nanofiller incorporation, with no evident variation in peaks width or angle position.

Figure 7 shows typical stress–strain curves for neat PLA and PLA/BC nanocomposites obtained in uniaxial tensile tests. It can be observed in this figure that neat PLA presented completely ductile behavior, characterized by the presence of a yield point followed by strain softening and a significant plateau before final fracture [67]. The nanocomposites, in contrast, displayed a more brittle behavior and failed after limited plastic deformation. Tensile parameters values are listed in Table 2 along with their deviations. Despite the well-known strength and stiffness of dried BC pellicles, the incorporation of unmodified BC into PLA was clearly detrimental to the material's tensile behavior. This was attributed to the aggregation of native BC nanoribbons within the PLA matrix described before, which hindered proper interfacial adhesion and load transfer. Modification of BC, on the other hand, led to improved filler dispersion and filler/matrix interaction, and hence, to some improvements

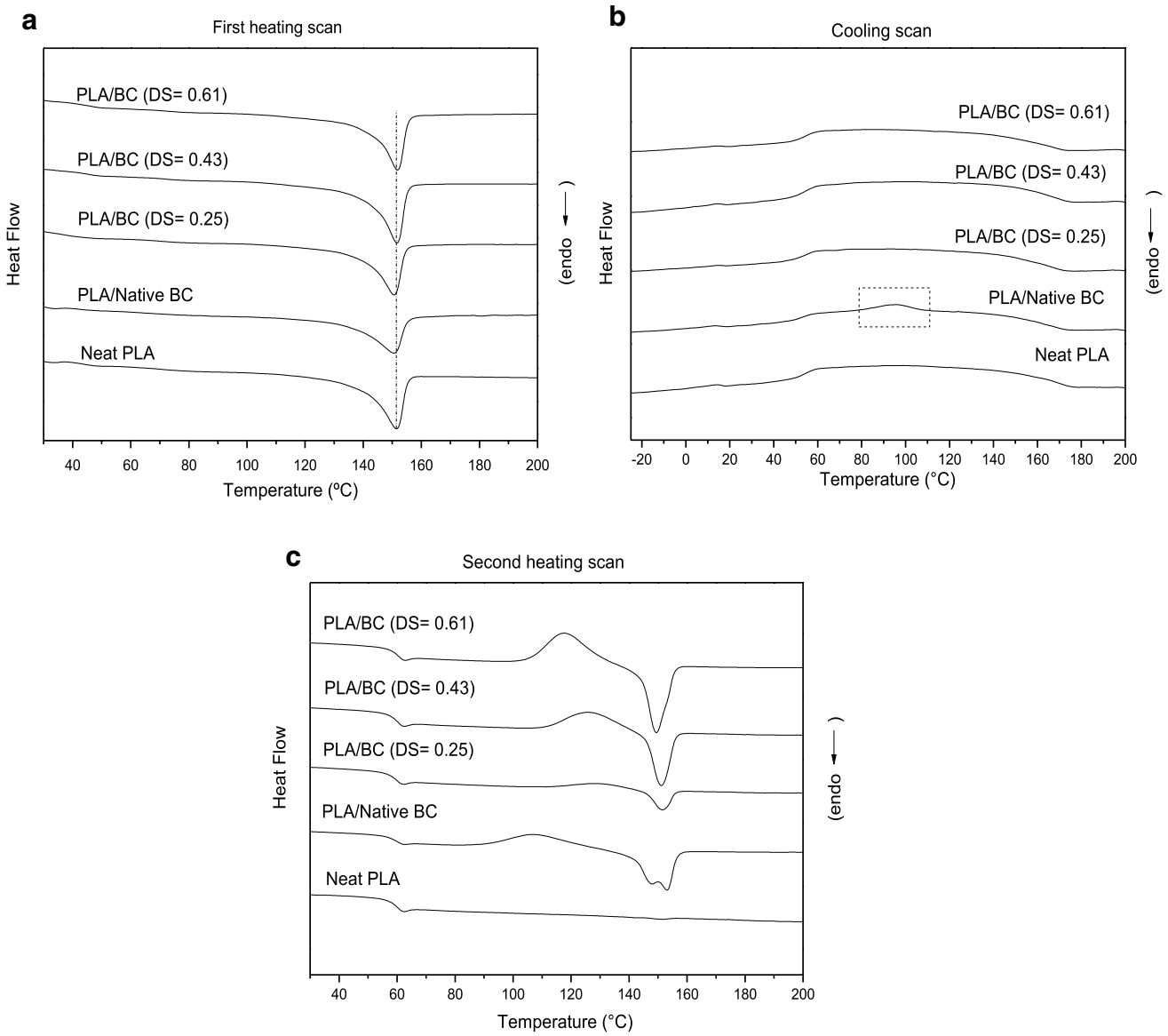

Fig. 5 DSC thermograms of neat PLA and PLA/BC nanocomposites. **a** First heating scan, **b** cooling scan, **c** second heating scan

Table 1 Thermal properties of neat PLA and PLA/BC nanocomposites

Sample	First heating scan			Cooling scan		Second heating scan	
	T_m (ºC)	ΔH_m (J/g)	X (%)	T_g (ºC)	T_{cc} (ºC)	T_{cc} (ºC)	T_m (ºC)
Neat PLA	151	32	35	59	–	–	–
PLA/native BC	151	34	36	59	96	107	149, 153
PLA/BC (DS = 0.25)	151	33	36	59	–	129	152
PLA/BC (DS = 0.43)	152	34	37	59	–	127	151
PLA/BC (DS = 0.61)	152	34	37	59	–	117	150

in tensile stiffness and strength. These improvements are similar to those reported in the literature for PLA/BC nanocomposites with the same range of filler content used here [28, 37, 38]. Ductility, characterized by strain at break values, was found to be significanlty lower in the nanocomposites respect to neat PLA, which is a consequence of

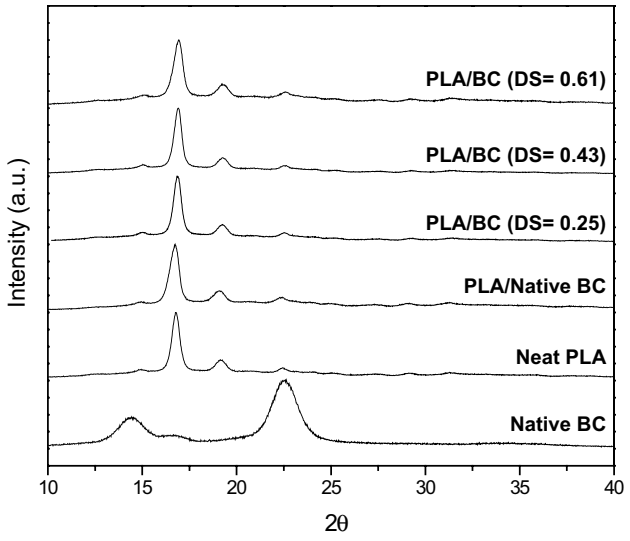

Fig. 6 X-ray diffraction data for native BC, neat PLA and PLA/BC nanocomposites

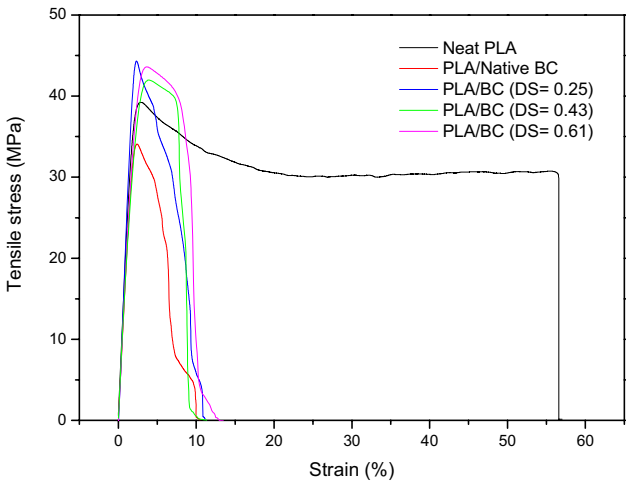

Fig. 7 Typical tensile stress–strain curves for neat PLA and PLA/BC nanocomposites

Table 2 Tensile parameters values for neat PLA and PLA/BC nanocomposites (Deviation between brackets)

Sample	Young's Modulus (MPa)	Tensile strength (MPa)	Strain at break (%)
Neat PLA	2221 (174)	40 (1)	51 (17)
PLA/native BC	1932 (124)	35 (2)	12 (7)
PLA/BC (DS = 0.25)	2480 (139)	45 (4)	11 (4)
PLA/BC (DS = 0.43)	2323 (135)	40 (2)	10 (5)
PLA/BC (DS = 0.61)	2542 (133)	46 (1)	9 (4)

the introduction of the stiffer filler into the ductile matrix [68]. However, and in accordance with previous data shown herein, no significant differences among the three DS investigated were observed in tensile parameters.

Conclusions

PLA nanocomposite films reinforced with native and acetylated bacterial cellulose were prepared. Acetylation of BC nanoribbons was performed by a non-conventional route in presence of citric acid. Manipulation of esterification time allowed obtaining BC with three different derivatization extents (i.e. DS), and in all cases surface-only acetylation of the nanofibers was observed.

PLA/BC nanocomposite films were produced by solvent casting and characterized by means of transparency analysis, FESEM, DSC, XRD and uniaxial tensile testing. Results evidenced the enhanced nanofiller dispersion accomplished upon derivatization of BC, as a result of better compatibility between nanocomposite components. However, no significant differences were observed among the different acetylation extents conferred to BC, suggesting that the minimum DS used (i.e. 0.25) was enough to reduce the repulsive forces between hydrophilic BC and less polar PLA and improve their interfacial contact. The results of mechanical properties further supported the described findings.

Overall, the non-conventional sustainable route proposed in this work to derivatize the surface of bacterial cellulose nanoribbons, seems to be a promising approach to obtain PLA/BC nanocomposites with reinforcement levels typically achieved for similar materials.

Acknowledgements Authors acknowledge Consejo Nacional de Investigaciones Científicas y Técnicas (CONICET- PIP 11220150100660) and Agencia Nacional de Promoción Científica y Tecnológica (PICT 2016-0843—PRESTAMO BID) for financial support.

Compliance with ethical standards

Conflict of interest The authors confirm that this article content has no conflict of interest.

References

1. Henton DE, Gruber P, Lunt J, Randall J (2005) Polylactic acid technology. In: Mohanty AK, Misra M, Drzal LT (eds) Natural fibers, biopolymers, and biocomposites. CRC Press, New York, pp. 527–577
2. Oksman K, Mathew AP, Bondeson D, Kvien I (2006) Compos Sci Technol 66:2776
3. Sanchez-García M, Lagaron J (2010) Cellulose 17:987
4. Fortunati E, Luzi F, Puglia D, Dominici F, Santulli C, Kenny JM, Torre L (2014) Eur Polym J 56:77

5. Hossain KMZ, Ahmed I, Parsons AJ, Scotchford CA, Walker GS, Thielemans W, Rudd CD (2012) J Mater Sci 47:2675
6. Jonoobi M, Harun J, Mathew AP, Oksman K (2010) Compos Sci Technol 70:1742
7. Kowalczyk M, Piorkowska E, Kulpinski P, Pracella M (2011) Compos A 42:1509
8. Wang Y, Drzal LT (2012) Appl Mater Interfaces 4:5076
9. Baheti V, Militky J, Mishra R, Behera B (2013) Text Sci Eng 3:130
10. Ghasemi S, Behrooz R, Ghasemi I (2017) J Bionanoscience 11:554
11. Kim Y, Jung R, Kim HS, Jin H-Y (2009) Curr Appl Phys 9:569
12. Luddee M, Pivsa-Art S, Sirisansaneeyakul S, Pechyen C (2014) Energy Proc 56:211
13. Quero F, Nogi M, Yano H, Abdulsalami K, Holmes S, Sakakini B, Eichhorn J (2010) J Appl Mater Interfaces 2:321
14. Panaitescu DM, Frone AN, Chiulan I, Gabor RA, Spataru IC, Casarica A (2017) BioResources 12:662
15. Lin N, Huang J, Chang PR, Feng J, Yu J (2011) Carbohydr Polym 83:1834
16. Fortunati E, Armentano I, Zhou Q, Puglia D, Terenzi A, Berglund LA, Kenny JM (2012) Polym Degrad Stab 97:2027
17. Fortunati E, Peltzer M, Armentano I, Torre L, Kenny JM (2012) Carbohydr Polym 90:948
18. Fortunati E, Armentano I, Zhou Q, Iannoni A, Saino E, Visai L, Berglund LA, Kenny JM (2012) Carbohydr Polym 87:1596
19. Robles E, Urrusola I, Labidi J, Serrano L (2015) Ind Crops Prod 71:44
20. Spinella S, Lo Re G, Liu B, Dorgan J, Habibi Y, Leclére P, Raquez J-M, Dubois P, Gross RA (2015) Polym J 65:9
21. Trifol J, Plackett D, Sillard C, Hassager O, Daugaard AE, Bras J, Szabo P (2016) J Appl Polym Sci 133:43257
22. Xu Ch, Lv Q, Wu D, Wang Z (2017) Cellulose 24:2163
23. Frone AN, Berlioz S, Chailan J-F, Panaitescu D (2013) Carbohydr Polym 91:377
24. Jonoobi M, Mathew AP, Abdi MM, Makinejad MD, Oksman K (2012) J Polym Environ 20:991
25. Habibi Y, Aouadi S, Raquez J, Dubois P (2013) Cellulose 20:2877
26. Song Z, Xiao H, Zhao Y (2014) Carbohydr Polym 111:442
27. Ambrosio-Martın J, Fabra MJ, Lopez-Rubio A, Lagaron JM (2015) Cellulose 22:1201
28. Lee K-Y, Blaker JJ, Bismarck A (2009) Compos Sci Technol 69:2724
29. Quero F, Eichhorn J, Nogi M, Lee K-Y, Bismarck A (2012) J Polym Environ 20:916
30. Tomé LC, Pinto RJB, Trovatti E, Freire CSR, Silvestre AJD, Neto CP, Gandini IA (2011) Green Chem 13:419
31. Zhang X, Li W, Ye B, Lin Z, Rong J (2013) J Thermoplast Compos 26:346
32. Tingaut P, Zimmermann T, Lopez-Suevos F (2010) Biomacromolecules 11:454
33. Almasi H, Ghanbarzadeh B, Dehghannya J, Entezami AA, Asl AK (2015) Food Packag Shelf Life 5:21
34. Missoum K, Belgacem MN, Bra J (2013) Materials 6:1745
35. Czaja WK, Young DJ, Kawecki M, Brown RM (2007) Biomacromolecules 8:1
36. Corujo VF, Cerrutti P, Foresti ML, Vázquez A (2016) Production of bacterial nanocellulose from non-conventional fermentation media. In: Puglia D, Fortunati E, Kenny JM (eds) Multifunctional polymeric nanocomposites based on cellulosic reinforcements. Elsevier Inc, Amsterdam, pp. 39–59
37. Lee K-Y, Bismarck A (2016) Bacterial nanocellulose as reinforcement for polymer matrices. In: Gama M, Dourado F, Bielecki S (eds) Bacterial nanocellulose from biotechnology to bio-economy. Elsevier, Chenai, pp 109–122
38. Panaitescu DM, Frone AN, Chiulan I (2016) Ind Crops Prod 93:251
39. Agustin MB, Nakatsubo F, Yano H (2016) Cellulose 23:451
40. Berlioz S, Molina-Boisseau S, Nishiyama Y, Heux L (2009) Biomacromolecules 10:2144
41. Blaker JJ, Walters K-YM, Drouet M, Bismarck A (2014) React Funct Polym 85:185
42. Cunha AG, Zhou Q, Larsson PT, Berglund LA (2014) Cellulose 21:2773
43. Suetsugu M, Kotera M, Nishino. MT, (2009) Cellulosic nanocomposite prepared by acetylation of bacterial cellulose using supercritical carbon dioxide. In: 17th International Conference on Composite Materials, 2009, Edinburgh, UK
44. Gonçalves S, Padrão J, Rodrigues IP, Silva JP, Sencadas V, Lanceros-Mendez S, Girão H, Dourado F, Rodrigues LR (2015) Biomacromolecules 16:1341
45. Hu W, Chen S, Xu Q, Wang H (2011) Carbohydr Polym 83:1575
46. Ifuku S, Nogi M, Abe K, Handa K, Nakatsubo F, Yano H (2007) Biomacromolecules 8:1973
47. Kim D, Nishiyama Y, Kuga S (2002) Cellulose 9:361
48. Lee K-Y, Quero F, Blaker JJ, Hill CAS, Eichhorn SJ, Bismarck A (2011) Cellulose 18:595
49. Lee K-Y, Bismarck A (2012) Cellulose 19:891
50. Tomé LC, Brandão L, Mendes AM, Silvestre AJD, Neto CP, Gandini A, Freire CSR, Marrucho IM (2010) Cellulose 17:1203
51. Tomé LC, Freire MG, Rebelo LPN, Silvestre AJD, Neto CP, Marrucho IM, Freire CSR (2011) Green Chem 13:2464
52. Yamamoto H, Horii F, Hirai A (2006) Cellulose 13:327
53. Ávila Ramírez JA, Juan Suriano C, Cerrutti P, Foresti ML (2014) Carbohydr Polym 114:416
54. Ávila Ramírez JA, Gómez Hoyos C, Arroyo S, Cerrutti P, Foresti ML, Curr ML (2016) Organocatal 3:161
55. Ávila Ramírez JA, Gómez Hoyos C, Arroyo S, Cerrutti P, Foresti ML (2016) Carbohydr Polym 153:686
56. Domínguez de María P (2010) ChemCatChem 2:487
57. Cerrutti P, Roldán P, Martínez García R, Galvagno MA, Vázquez A, Foresti ML (2016) J Appl Polym Sci 133:43109
58. Hestrin S, Schramm M (1954) Biochem J 58:345
59. Ilharco LM, Gracia RR, da Silva JL, Ferreira LFV (1997) Langmuir 13:4126
60. Segal L, Creely JJ, Martin AE, Conrad CM (1959) Text Res J 29:786
61. Turner JF, Riga A, O`Connor A, Zhang J, Collis J (2004) J Therm Anal Calorim 75:257
62. Haigler CH. Read, alteration of cellulose assembly in *Acetobacter xylinum* by fluorescent brightening agents, direct dyes and cellulose derivatives (University of North Carolina at Chapel Hill, 1982)
63. Hirai A, Tsuji M, Yamamoto H, Horii F (1998) Cellulose 5:201
64. Gan K, Nechwatal A, Frankenfeld K, Schlufter K (2012) J Compos Mater 2:97
65. Dai X, Cao Y, Wang X (2016) RSC Adv 6:71461
66. Teixeira EM, de Campos A, Marconcini JM, Bondancia TJ, Wood D, Klamczynski A, Mattoso LHC, Glenn GM (2014) RSC Adv 4:6616
67. Young RJ, Lovell PA (1991) Introduction to polymers, Chap. 5 2nd edn. Chapman and Hall, London
68. Pérez E, Famá L, Pardo SG, Abad MJ, Bernal C (2012) Composites B 43:2795